Plasmonic nanodiamonds : targeted coreshell type nanoparticles for cancer cell thermoablation

Plasmonic Nanodiamonds – Targeted Core-shell Type Nanoparticles for Cancer Cell Thermoablation

Ivan Rehor[1], Karin L. Lee[2], Kevin Chen[2], Miroslav Hajek[1], Jan Havlik[1], Jana Lokajova[1], Milan Masat[1], Sourabh Shukla[2], Hamed Heidari[3], Sara Bals[3], Nicole F. Steinmetz[2,4,5,6], Petr Cigler[1,]**
* corresponding authors

[1]Institute of Organic Chemistry and Biochemistry, v.v.i., The Academy of Sciences of the Czech Republic, Flemingovo nam. 2, 166 10 Prague 6, Czech Republic.

Department of [2]Biomedical Engineering, [4]Radiology, [5]Materials Science and Engineering, [6]Macromolecular Science and Engineering, Case Western Reserve University, Schools of Medicine and Engineering, 10900 Euclid Avenue, Cleveland, OH 44106, USA.

[3]EMAT, University of Antwerp, Groenenborgerlaan 171, B-2020 Antwerp, Belgium

Acknowledgements
I. Rehor and K. L. Lee contributed equally to this work. This work was supported by GACR project P108/12/0640, MSMT CR grant no. LH11027, the National Science Foundation, CMMI NM 333651 (to NFS), a NCI R25 CA148052 Cancer Pharmacology training grant (KLL), and NPU I project LO 1302 from Ministry of Education (MH). Part of this work was performed within OPPK project CZ.2.16/3.1.00/24016. S.B. acknowledges financial support from the European Research Council (ERC Starting Grant #335078-COLOURATOMS).

Abstract
Targeted biocompatible nanostructures with controlled plasmonic and morphological parameters are promising materials for cancer treatment based on selective thermal ablation of cells. Here, core–shell plasmonic nanodiamonds consisting of a silica-encapsulated diamond nanocrystal coated in a gold shell are designed and synthesized. The architecture of particles is analyzed and confirmed in detail using electron tomography. The particles are biocompatibilized using a PEG polymer terminated with bio-orthogonally reactive alkyne groups. Azide-modified transferrin is attached to these particles, and their high colloidal stability and successful targeting to cancer cells overexpressing the transferrin receptor are demonstrated. The particles are nontoxic to the cells and they are readily internalized upon binding to the transferrin receptor. The high plasmonic cross section of the particles in the near-infrared region is utilized to quantitatively ablate the cancer cells with a short, one-minute irradiation by a pulse 750-nm laser.

1. Introduction
Plasmonic nanostructures (PNs) of various shapes and composition [1,2] have garnered scientific interest in recent years due to their unique optical properties, which allow their use for construction of therapeutic and theranostic nanoparticles, bioprobes, and sensors. [1,3] For a nanosized noble metal particle, the de Broglie wavelength of the valence electrons is of the same order of magnitude as the size of the particle, and quantum size effects may appear. The valence electrons then start to oscillate at a collective oscillation frequency, giving rise to characteristic plasmon resonance bands. [3,4] Because of these properties, PNs gained interest in the fields of biotechnology and biomedicine. Through nanostructure design, their plasmonic absorption wavelength can be finely tuned to fall in the near-infrared tissue imaging window (650–900 nm) where light can penetrate up to a few centimeters into the tissue. The huge absorption and scattering of PNs enables their use as a contrast agent for optical imaging of tissues, e. g., in optical coherence tomography [5,6] or photoacoustic [7] imaging. Furthermore, the absorbed light is transformed into heat, allowing for use of PNs in cancer therapy. [8–10] The heat may be used for thermal ablation of tumors or to control the release of therapeutics, which are usually but not exclusively, [11] attached to the PN surface. [12] Merging diagnostic

imaging ability with a therapeutic function in one so-called “theranostic” agent is indeed promising, as evidenced by numerous recent publications addressing the topic. [13,14]

Here, we describe preparation of a plasmonic gold nanoshell (GNS) around silica-encapsulated diamond nanocrystals. Nanodiamonds (NDs) are highly biocompatible materials with applications in nanomedicine [15] and bioimaging. [16–19] Previous studies on gold plasmonic structures connected with diamonds were performed primarily on macroscopic substrates. [20–25] They have focused mainly on the photophysics of fluorescent nitrogen-vacancy centers embedded in a diamond crystal lattice. Creation of a well-defined plasmonic system on a single diamond nanoparticle in solution is limited by the colloidal instability of NDs in aqueous buffers. [26] To date, only direct covalent attachment of gold nanoparticles to NDs has been achieved, [27,28] and materials with unordered structural morphology [29,30] have been prepared.

We took advantage of our recently published methodology for silica coating of NDs, [31] which enables the creation of a well-defined plasmonic material based on a ND dielectric core coated with a GNS. We chose the core-shell design because it provides an extremely high plasmonic absorption cross section, as well as the possibility to tune the position of the absorption maximum within the near-infrared region, where light is minimally absorbed and scattered by the tissue. As a first step to demonstrate the utility of this newly constructed biomaterial in nanomedical applications, we show that it can be stabilized and rendered biocompatible by addition of PEG-containing ligands bearing bioorthogonally reactive alkyne groups, followed by decoration with synthetically modified transferrin (Tf). We use these particles to target cancer cells, which overexpress the Tf-receptor, and thermally ablate them by irradiation with a near-infrared pulse laser.

2. Results and Discussion

2.1. Preparation and Characterization of Particles

Creation of GNSs with a diamond core was achieved via multistep encapsulation, as depicted in Figure 1 A. Commercially available ND particles (Figure 1 B) are of irregular shape (circularity ~0.67) with sharp edges and often appear elongated in one dimension (needle–like). Their size distribution is broad, ranging from several nm to more than 50 nm in diameter. Therefore, before the GNS is generated on the ND surface, the particle shape needs to be normalized to spherical, and the size distribution should be narrowed. We achieved this through encapsulation of NDs in a silica shell, approximately 20 nm thick, using a method we described earlier. [31] The formation of the desired architecture was confirmed at each step by transmission electron microscopy (TEM), as shown in Figure 1 B-E. After coating with silica (Figure 1 C), the particles became more spherical (circularity ~0.87), and their diameter increased to 66 ± 10 nm. These pseudospherical silica-coated NDs (ND@ Sil) are suitable for encapsulation with a GNS, according to a procedure introduced by Halas and collaborators. [32,33] First, small gold nanoparticles (2–3 nm in diameter) were electrostatically anchored onto the silica particle surface (Figure 1 D). These assemblies were exposed to a reductive environment containing gold(III) ions, which served as nucleation centers for GNS growth (Figure 1 E). The growth of shells ended after several tens of seconds, yielding a deep blue solution containing GNS-coated NDs (ND@Au).

To investigate the structure and thickness of these GNSs in detail, we analyzed individual ND@Au particles using HAADFSTEM electron tomography. This technique yields images in which the intensity approximately scales with the square of the atomic number of the elements present in the region of interest. Due to the limited dynamic range of the HAADF detector, maintaining similar intensities for Au and silica in the projection images is not feasible because of the large differences in atomic number. We therefore focused on 3-dimensional reconstruction of GNSs. In Figure 2 A–C, 2-dimensional projections of a GNS imaged at different angles are presented. The 3-dimensional reconstruction resulting from the electron tomography experiment is presented in Figure 2 D and E. The shell thickness is mostly homogenous. We evaluated the average shell thickness as 12.6 ± 0.3 nm, and the total internal surface of the GNS was 32 600 nm 2 . The intermittent presence of small holes is likely caused by incomplete filling of the spaces between individual seeds with gold.

The formation of the GNS is reflected in absorption spectra by a characteristic broad plasmonic band with an absorption maximum at 675 nm (Figure 2 G). The position of the maximum corresponds to values published for silica particles coated with GNSs of similar sizes and thicknesses. [34]

2.2. Introduction of Protective and Bioorthogonally Reactive PEG Coating

The application of GNS-based materials in living systems requires their protection against ionic-strength-induced aggregation/ precipitation in buffers and biological liquids, as well as against opsonization. Poly(ethylene oxide) (PEG) is an effective polymeric bio-nanointerface, shielding particles against these factors, rendering them “stealth” to the immune system, and prolonging their circulation in the body. [35] In addition to these attributes, PEG can serve as heterobifunctional linker to connect nanoparticles with attached moieties. For functionalization of ND@Au , we utilized mid-size PEG (5 kDa) terminated with lipoic acid at one end and an aliphatic alkyne at the other (Figure 3 A). Lipoic acid serves as an instant anchoring group, possessing stronger and more stable interaction with gold than terminal aplihatic thiols. [36] Of the available bioconjugation

techniques, we chose Cu(I)-catalyzed Huisgen alkyne-azide cycloaddition (click reaction) because of its high orthogonality with other reactive groups in biomolecules and excellent conjugation yields in aqueous solution even at very dilute concentrations. [37] To analyze the effect of PEG protection on the colloidal stability of particles, we performed comparative stability tests of PEG-modified GNSs (ND@Au-PEG) and unmodified ND@ Au . We exposed the particles to different aqueous solutions with high ionic strength and monitored the hydrodynamic radii over time by dynamic light scattering. While PEG-protected ND@Au-PEG exhibited unlimited colloidal stability in PBS, physiological solution (0.15 M NaCl) and cell growth media (RPMI media + serum) (Figure 3 B), naked ND@Au particles immediately agglomerated and precipitated from the buffers (Figure 3 C), with the exception of cell growth media. The particles remained stable in media, most likely due to formation of a protein corona by adsorption of proteins from serum.

2.3. Modifi cation of Particles with Alexa Fluor 647 and Transferrin

For cancer cell targeting experiments, we selected human holotransferrin (Tf), a glycoprotein that is internalized into cells via clathrin-mediated endocytosis upon binding to Tf receptors (TfR). TfR are expressed in negligible numbers on non-dividing cells, but are highly upregulated on rapidly dividing cancer cells, reaching expression levels of up to 10 5 Tf-R per cell. [38] This makes Tf a suitable targeting ligand to direct nanomaterials, such as ND@Au , to cancer cells. This general approach has been successfully demonstrated for various nanoparticles, [39] such as virus-like particles, [40] liposomes [41] and nanodiamonds. [42,43] To ensure protein reactivity for the click bioconjugation strategy, we introduced azide groups to the protein. As previously described, [44] Tf offers a favorable pathway for selective derivatization: a reactive aldehyde can be produced by mild periodate cleavage of 1,2-diols on sialic acid (N –acetyl neuraminic acid) moieties present in the Tf glycosylation pattern. We derivatized the obtained aldehydes with aminooxypropylazide, a “clickable” heterobifunctional linker that forms a physiologically stable aldoxime (for structures, see Figure 3 A). Compared to ligation via amino or thiol groups, this approach results in better control over protein attachment points, because one Tf molecule contains only four sialic acids residues at well-defined and sterically accessible positions. [44]

To obtain fluorescent particles, which enable quantification of targeting by flow cytometry and analysis of the particles’ subcellular localization by confocal microscopy, we first reacted the alkyne-bearing ND@Au-PEG particles with Alexa Fluor 647- azide, yielding fluorescent ND@Au-nT conjugate. Although gold plasmonic systems can quench emission from fluorescent dyes, [45] the dye in this case remained fluorescent and was observable with both flow cytometry and confocal microscopy. Linear PEG with a molecular weight of 5000 Da has a Flory dimension of ≈6.0 nm in solution; [46] it is therefore anticipated that the PEG spacer placed between the plasmon surface and fluorophore will effectively shield the quenching effects. The number of Alexa Fluor 647 molecules per particle, however, was difficult to estimate because of the strong interference of particles’ plasmonic properties and the extinction and emission fluorescence bands of the dye. As a next step, we attached azide modified Tf to unreacted alkyne groups of ND@Au-nT under similar conditions, providing ND@Au-Tf .

2.4. Targeting of Cancer Cells

Target-specificity and cellular uptake of particles was evaluated in TfR-expressing SKBR3 cells (a human breast cancer cell line) using flow cytometry (quantitative) and confocal microscopy (qualitative). Flow cytometry indicated that both types of particles, ND@ Au-nT and ND@Au-Tf , bound to the cells, with the Tf-targeted preparation ND@Au-Tf showing enhanced interactions. Our data indicate that 26% of the cell population was targeted by ND@Au-Tf , while non-specific uptake was attributed to 18% of the cells, as indicated by ND@Au-nT-cell interactions ($p < 0.05$, Figure 4). Cell targeting properties were found to be reproducible in other cell lines, such as HeLa cells (not shown). Competition binding assays using free Tf ligand further confirmed the target-specificity of the ND@Au-Tf conjugate. Competition with a molar excess of 5:1 or 20:1 Tf:ND@Au-Tf particles resulted in reduced cell uptake, with levels comparable to those observed for non-targeted ND@Au-nT. This indicates that the ND@Au-Tf particles indeed target the cells, and binding can be attributed to specific interactions between Tf-R and ND@Au-Tf (Supporting Information Figure S2). Next, we sought to investigate the cellular fates of ND@Au-Tf and ND@Au-nT , specifically addressing whether the ND formulations would be taken up into cells. Cell membranes and nuclei were stained, and Z-stacked (0.3 micrometer/steps) confocal images were recorded. Data indicate that after a 3-hour incubation period, both ND@Au-Tf and ND@Au-nT formulations were bound to cell membranes (data not shown). Interestingly, after a 16-hour incubation period, ND@Au-Tf appeared intracellularly, whereas ND@Au-nT particles co-registered with the cell membrane (Figure 5), indicating that although both formulations are able to bind to cellular membranes, only ND@Au-Tf are internalized. Because our cell binding studies showed that ND@Au-Tf particles specifically bind TfR, ND@Au-Tf internalization is likely mediated by TfR endocytosis. Co-localization studies were carried out, further indicating that non- targeted ND@Au-nT are co-localized with the cell membrane with Mander's coefficient $M2 = 0.99$. In stark contrast, only a fraction of the targeted ND@Au-Tf formulation remained bound to the cell membrane ($M2 = 0.21$), while the remainder translocated inside the cell. Our flow

cytometry and confocal imaging results are in agreement, and the data support ND@Au-Tf targeting of TfR on cancer cells, leading to receptor-mediated internalization.

2.5. Toxicity Study

The toxicity of the ND@Au-Tf particles themselves was investigated in SKBR3 cells, using an XTT cell proliferation assay. After 3- or 24-hour incubation with ND@Au-Tf particles, we did not observe significant differences in cell viability compared to non-treated cells, indicating that ND@Au-Tf particles are not cytotoxic (Supporting Information Figure S3).

2.6. Laser Ablation

The ability of GNSs to kill cancer cells upon red laser irradiation was demonstrated in vitro. HeLa cells were incubated with Nd@Au-Tf , and after successive washing, irradiated with a Ti:Sapphire pulse laser. After a one-minute irradiation, cells were incubated for 24 hours, and their viability was estimated using luciferase assay (Figure 6). Exposing HeLa cells to ND@ Au-Tf did not affect their viability, supporting the non-toxicity of these particles. Laser irradiation of cells also had no influence on their viability. Only cells exposed to both nanoparticles and laser were affected and—after only one minute of irradiation—completely killed. The laser power we used (37 W/cm^2) was of the same order of magnitude as values described in the literature for in vitro experiments. [9,10,47]

3. Conclusion

In summary, we synthesized a novel plasmonic nanomaterial consisting of a diamond core coated with a silica layer and encapsulated with a thin GNS. PEG chains were attached to the surface of GNSs using lipoic acid as an anchor. The other ends of the PEG chains were further functionalized with Alexa Fluor 647 and modified transferrin via click chemistry. Transferrin-labeled NDbased GNSs (ND@Au-Tf) target transferrin receptors, which are overexpressed on many cancer cell types. We found that ND@Au-Tf bind and are internalized into human SKBR3 breast cancer cells and HeLa cervical cancer cells. Cell viability assays were also conducted using XTT assay; toxic effects were not observed after 3- or 24-hour incubation periods. We also demonstrated the ability of the prepared GNSs to kill cancer cells upon red laser irradiation in vitro. HeLa cells were completely killed after a one-minute irradiation with a pulse 750-nm pulse laser (37 W/cm 2), while no harm was caused to cells by irradiation itself or by the presence of GNSs without irradiation. This work lays the foundation for the multi-step synthetic route leading to ND core plasmonic nanoparticles and is the first stepping stone toward translational research. Future work will focus on targeted therapeutic studies of plasmonic NDs in vivo. Specifically, studies will set out to gain an understanding on the therapeutic efficacy in the context of biodistribution and overall biocompatibility of the materials. At the same time, studies will assess the photophysical interactions of the fluorescent nitrogen-vacancy (NV) centers in NDs with the gold plasmonic shell. It is well recognized that cancer nanotechnology holds great promise in modern medicine, and several nanoparticles have advanced into clinical application. [48–50] While the development pipeline with new nanomaterial-based technologies is moving rapidly, the fundamental understanding of the nanomaterial's in vivo fate; i.e., the biodistribution, clearance or persistence, pharmacokinetics and pharmacodynamics, is often lacking. However, detailed understanding of the biological behaviour, the interplay of tissue-targeting and immune surveillance in the context of imaging sensitivity and therapeutic efficacy, is imperative for rapid clinical viability and success of plasmonic nanostructures. [51] The combined knowledge of the biological properties and diagnostic/therapeutic potential will help identify a suitable nitch application harnessing the unique properties of the proposed material.

4. Experimental Section

Chemicals and Solvents: The NHS ester of lipoic acid was prepared according to a previously published procedure. [52] H 2 N-PEG(5000)-alkyne was purchased from Iris Biotech. Alexa Fluor 647-azide was purchased from Invitrogen. Tetrakis(hydroxymethyl)phosphonium chloride (THPC) and tetraethyl orthosilicate (TEOS) were purchased from Sigma-Aldrich. HAuCl 4 was purchased from Alfa Aesar. UV–Vis Spectroscopy : The spectra were recorded with a Specord 210 (Analytik Jena) spectrometer in the 400–1000 nm range at room temperature with an optical path of 1 cm.

Dynamic Light Scattering: For stability studies in buffers, DLS was recorded with a Zetasizer Nano ZS system (Malvern Instruments) at 25 °C. The particle concentration was 0.3 mg/mL (10 μg ND/mL).

Electron Microscopy: Bright field TEM experiments were performed with a JEOL JEM-1011 electron microscope operated at 60 kV and equipped with a Veleta side-mounted camera. Carbon coated grids (Pyser) were used in all cases. Nanodiamond samples were prepared according to a previously published procedure. [53] Other samples were prepared as follows: a 3 μL droplet of particle dispersion (0.2 mg/mL) was placed on the grid and gently removed with a piece of tissue after 1 min incubation. Tilt series of 2-dimensional projection images for electron tomography were acquired using a FEI Tecnai G2 transmission electron microscope operated at 200 kV in scanning transmission electron microscopy (STEM) mode. To prepare the samples, a drop of diluted colloidal solution was placed on a carbon-coated copper grid and left to dry. The high angle

annular dark-field (HAADF-STEM) image series was acquired using a single tilt tomography holder (Fischione 2020) over the angular range (–64°,+76°) with step increments of 2°. The alignment and 3D reconstruction were carried out with FEI Inspect3D software. Quantification of the 3D data was performed using MATLAB codes.

Synthesis of LA-PEG-alkyne: Synthesis was performed according to published procedures, [36,54] with some modifications. Briefly, H 2 NPEG(5000)-alkyne (50 mg, 10 μmol) was dissolved in DCM (1 mL) and mixed with LA-NHS (50 mg, 165 μmol). The reaction mixture was stirred overnight, then washed 3 times with 10 mL hot water. The combined aqueous fractions were purified using a Millipore Ultracel 3K separation tube (washed 3 times with 20 mL water). TLC: MeOH:trimethylamine 100:5 (R f = 0.5), visualized with Co(NCS) x and KMnO 4 (no reaction with ninhydrin). H 2 N-PEG(5000)-alkyne R f < 0.3, visualized with ninhydrin and Co(NCS) x (no reaction with KMnO 4). 1 H NMR (400 MHz, CDCl 3 , δ): 1.6 (m, 2H), 1.7–1.9 (m, 3H), 2.0 (m, 1H), 2.1 (t, 1H, J = 3.6 Hz), 2.2–2.4 (m, 4H), 2.5 (t, 2H, J = 7.2 Hz), 2.6 (m, 3H), 3.2–3.3 (m, 2H), 3.5–3.9 (m, 240H), 3.9 (t, 1H, J = 5.2).

4.1. Transferrin-Azide (Tf-Azide)

Preparation: (see Figure 3 A) We used a procedure similar to that previously described for preparation of transferrin-alkyne. [44] NaIO 4 solution was slowly added to a cooled solution of human holotransferrin (30 mg, 390 nmol; 2 mg/mL) in acetate buffer (0.1 M , pH 5.5) to a fi nal NaIO 4 concentration of 1 m M . The mixture was incubated on ice in the dark for 30 min. The solution containing Tf-aldehyde was concentrated six times in an ultrafiltration cell (from 70 mL to 5 mL). HEPES buffer (0.1 M pH 7.2) was used to refill the volume. Tf-aldehyde was incubated with 3-aminooxypropyl-1-azide (16.2 mg, 140 μmol) in HEPES buffer with dimethyl sulfoxide (DMSO, 20%, total volume of 17 mL) for 5 h at room temperature with gentle mixing. Removal of excess 3-aminooxypropyl-1-azide was performed by ultrafiltration (70 mL to 5 mL, repeated six times) in HEPES buffer (0.1 M , pH 8). The solution was freeze-dried to obtain Tf-azide .

Characterization: The presence of a reactive azide group in Tf-azide was tested by reaction with fluorescein-alkyne. All solutions were aqueous except the fluorescein-alkyne stock, which was prepared in DMSO. The solutions were mixed to achieve the following final concentrations: 0.02 m M Tf-azide , 0.075 m M fluorescein-alkyne, 0.17 m M CuSO 4 ·5H 2 O, 0.33 m M tris(3-hydroxypropyltriazolylmethyl) amine (THPTA), and 5 m M sodium ascorbate. The solutions of CuSO 4 ·5H 2 O and THPTA were premixed (in a 1:2 molar ratio) before adding to the reaction mixture. The reaction mixture was well-sealed after adding sodium ascorbate, mixed, and reacted for 2 h with no stirring. The reaction product (Tf-Fl) was analyzed by SDS-PAGE (for details, see ESI). All samples (Tf , Tf-azide , and Tf-Fl) were of the same molecular weight, and only Tf-Fl can be seen under UV-lamp (Supporting Information Figure S1).

4.2. Nanoshell Preparation

Silica Encapsulation: NDs were solubilized in a manner similar to that described in commonly used procedures. [16,55] Briefly, NDs were treated with a mixture of HNO_3 and H_2SO_4 (85 °C, 3 days), washed with 2 M NaOH and 2 M HCl, washed five times with water, and freeze-dried. Prior to use, the particles were dissolved in water (2 mg/mL) and sonicated with a probe (Cole-Parmer, 750 W) for 30 min. The resulting transparent colloid was filtered using a 0.2 μm PVDF microfilter to provide a colloidal solution of ND particles. A modified version [31] of previously described general procedure [56] was used to coat NDs with silica shells. Polyvinylpyrrolidone (96 mg, 9.6 μmol) was dissolved in water (204 mL) and sonicated for 10 min in an ultrasonic bath. ND colloid (6 mL, 2 mg/mL) was added, and the mixture was stirred for 24 h. The colloid was then concentrated via centrifugation in two steps. In the first step (40 000 rcf, 1 h), the volume was reduced to approximately 12 mL. The second centrifugation step (30 000 rcf, 30 min) was performed in microvials and reduced the solvent volume to approximately 0.4 mL. Sedimented NDs were resuspended in ethanol (12 mL) in a round bottom flask and sonicated in an ultrasonic bath for 2–4 min. TEOS (112 mg, 539 μmol) was added. After 2 min of vigorous stirring, ammonia solution (25%, 500 μL) was added, and the reaction mixture was stirred for 14 h, affording silica-coated particles ND@Sil . The product was purified by centrifugation (14 000 rcf, 5 min) with ethanol (12 mL, 4×) and MeCN (12 mL, 2×) and was dissolved in 6 mL MeCN. ND@Sil particles were stored in the freezer (–18 °C) as a stable colloid for several months without changes in particle characteristics (confirmed with TEM and DLS) or reactivity.

GNS Formation: GNSs were prepared according to modified published procedures. [32–34] First, seeding gold colloid was prepared. Water (45 mL) was mixed with NaOH (5 mL, 0.1 M). Tetrakis(hydroxymethyl) phosphonium chloride (THPC, 67.2 μmol in 1 mL water) was added. After exactly 5 min, $HAuCl_4$ solution (2 mL of a 1% w/w solution in water, 59 μmol) was added in one portion under vigorous stirring. The mixture was stirred for 10 min, and the resulting gold colloid was aged at 4 °C for 2 weeks without purification. ND@Sil particles (1 mL MeCN dispersion, 2 mg ND content, 8 mg total ND@Sil weight) were mixed with 2-week aged gold colloid (30 mL). The pH of the mixture was adjusted to 3. The mixture was gently stirred for 20 min and then kept at 4 °C for 16 h. ND@Sil particles coated with gold seeds were isolated by centrifugation (2500 rcf, 1 h) and washed twice with water (30 mL, isolated at 2500 rcf, 1 h). The volume of the dispersion was adjusted to 5 mL. K_2CO_3 (200 mg, 1.44 mmol) was dissolved in 800 mL water, and $HAuCl_4$ solution (12 mL of a 1% w/w solution in water, 3.5 μmol) was added.

The solution was stirred for 24 h in the dark. Then, the pH of the solution was adjusted to 9.0. Gold-seeded ND@Sil dispersion (1.25 mL; 0.5 mg ND content) was added to 200 mL solution. A stream of CO was bubbled through the solution for 2 min under vigorous stirring. The color changed from transparent to red, purple, and then dark blue. Gold encapsulated ND@Sil (ND@Au) were separated by centrifugation at 20 rcf overnight and concentrated to 2.5 mL. The total mass of ND@Au particles obtained in one run was on average 15 mg, i.e., 30-fold the mass of ND and 7.5-fold the mass of ND@Sil .

PEGylation of ND@Au: LA-PEG-alkyne (10.3 mg, 2 μmol) was added to ND@Au dispersion (15 mg; corresponds to 0.5 mg ND) in 2.5 mL water. The mixture was sonicated in an ultrasonic bath for 20 min, then stirred overnight and sonicated for another 20 min. PEG-coated ND@Au particles were separated by centrifugation (5×, 500 rcf, 20 min), yielding ND@Au-PEG.
Modification with transferrin and Alexa Fluor 647: A solution of Cu-catalyst was prepared in a separate vial by mixing $CuSO_4 \cdot 5H_2O$ (20 μL of a 25 m M solution) and THPTA ligand (20 μL of a 50 m M solution).The click reactions were performed similarly to those described in the literature [57] by mixing reactants in a 0.6 mL vial. ND@Au-PEG solution (1.5 mg particles in 125 μL) was mixed with a DMSO solution of Alexa Fluor 647-azide (1.7 μL of a 5.88 m M solution). Other components were added in the following order and quantities: aminoguanidine hydrochloride (12 μL of a 100 m M solution) and Cu-catalyst solution (3.2 μL) (see above). Water was added to adjust the total reaction volume to 200 μL. Sodium ascorbate (12 μL of a 100 m M solution) was added. The vials were well-sealed and kept for 2 h without stirring or shaking. Modified nanoparticles were isolated in near-quantitative yield by centrifugation (500 rcf, 20 min) and washed with water (2×, 1 mL) and PBS (1×, 1 mL) to yield gold-coated NDs tagged with Alexa Fluor 647 (ND@Au-nT). ND@Au-nT was further modified with Tf-azide in a similar manner. Solid Tf-azide (0.2 mg) was added to nanoparticles, and other components were added in the same quantities and order as in the previous reaction step. After centrifugal separation, ND@Au-Tf was obtained.
Stability Experiments: A colloidal aqueous solution of ND@Au-PEG (1.5 mg/mL, 100 μL) was added to buffer (900 μL). The following buffers were used: PBS (pH = 7.5), 0.15 M NaCl, 0.3 M NaCl, and cell growth medium (RPMI-1640 + serum). The samples were stored at 25°C, and the aggregation state was examined with DLS 2 h, 1 day, and 1 month after mixing. Ten minutes before each measurement, samples were sonicated in a bath for 20 s.

4.3. Cell Studies

Flow Cytometry : SKBR3 cells were cultured in McCoy's 5A media supplemented with 10% (v/v) fetal bovine serum (FBS), 1% (v/v) penicillin-streptomycin, and 1% (v/v) L-glutamine at 37 °C and 5% CO_2 (all reagents were obtained from Invitrogen). Cells (100 000 cells/500 μL media/well) were added to untreated 24-well plates and incubated overnight. The following day, triplicates of i) culture medium alone (negative control), ii) gold-coated NDs tagged with Alexa Fluor 647 (ND@Au-nT), and iii) gold-coated NDs tagged with Alexa Fluor 647 and transferrin (ND@Au-Tf) were added. Particle concentrations were approximately 1×10^{12} particles/mL (1.2 mg particles per 1 mL, 300 μL fi nal volume; 3×10^6 particles/cell) in culture medium. Particles were incubated with cells for 3 h. (Competition binding assays were also carried out: ND@Au-Tf were incubated with free Tf added to the medium in a molar excess of 5:1 or 20:1, see Supporting Information). Following incubation, cells were washed three times with 0.09% (w/v) saline to remove non-bound particles remaining in solution. Cells were removed using 200 μL enzyme-free Hank's based cell dissociation buffer (Gibco), added to untreated 96-well v-bottom plates, and centrifuged at 500 g for 4 min. The supernatant was removed. Cells were then washed in FACS buffer (0.1 mL of 0.5 M EDTA, 0.5 mL FBS, and 1.25 mL of 1 M HEPES, pH 7.0, in 50 mL Ca 2+ - and Mg 2+ -free PBS). Washing was repeated twice. Cells were fixed in 2% (v/v) paraformaldehyde in FACS buffer at room temperature for 10 min and washed twice. Samples were analyzed using a BD LSR II flow cytometer, with a total of 10,000 gated events collected per sample. FlowJo 10.0.00003 software was used for data analysis.
Confocal Microscopy: SKBR3 cells (25 000 cells/500 μL media/well) were added to coverslips, which were placed in untreated 24-well plates and incubated overnight. The following day, duplicates of i) no particles, ii) ND@Au-nT , and iii) ND@Au-Tf were added at concentrations of approximately 1×10^{12} particles/mL (1.2 mg particles per 1 mL, 300 μL final volume, 1.2×10^7 particles/cell) and incubated with the cells for 16 h. Following incubation, cells were washed three times with 0.09% (w/v) saline to remove excess particles. Samples were fixed in 5% (v/v) paraformaldehyde and 0.3% (v/v) gluteraldehyde in Dulbecco's PBS (Fisher) for 10 min at room temperature. Cells were blocked in 5% (v/v) goat serum (Invitrogen) for 90 min at room temperature. Cell membranes were stained using 1 μg/mL wheat germ agglutinin-A555 (Invitrogen) and 1% (v/v) goat serum in Dulbecco's PBS for 45 min at room temperature. Cell nuclei were stained using 4'6'-diamidino-2- phenylindole (DAPI) (MP Biomedicals) diluted 1:9,500 in Dulbecco's PBS for 15 min at room temperature. In between each step, cells were washed three times with Dulbecco's PBS. Slides were mounted using Permount mounting media (Fisher). Confocal analysis was performed using the Olympus FV1000 laser scanning confocal microscope and a 40x objective. Images were analyzed using ImageJ 1.43u software.

XTT Cell Proliferation Assay: SKBR3 cells (25,000 cells, 200 μL media per well) were added to 96-well plates and incubated at 37 °C under 5% CO_2 overnight. The following day, ND@Au-Tf particles were added at a concentration of approximately 1 ×

10^{12} particles/mL (1.2 mg particles per 1 mL, 75 μL final volume, 3×10^6 particles/cell); control cells with no added particles were also set up. Following a 3 or 24 h incubation, wells were washed three times with 0.09% (w/v) saline to remove unbound NDs. Then, 200 μL fresh media was added, and cells were returned to incubate for an additional 24 h. An XTT cell proliferation assay (ATCC) was used to assess cellular viability; the protocol was performed according to the manufacturer's instructions. A Tecan Infinite 200 plate reader was used to measure the absorbance, and percent viability was determined by normalizing to the cell-only control.

Laser Ablation Experiments: Human cervical adenocarcinoma (HeLa) cells (ATCC® CCL-2™) were cultured in RPMI 1640, Dutch modification medium supplemented with 10% (v/v) heat-inactivated fetal bovine serum (FBS), antibiotics (200 μg/mL streptomycin and 100 U/mL penicillin G) and 2 mM glutamine (all purchased from Sigma-Aldrich) at 37°C in a humidified atmosphere containing 5% CO 2 . Cells were subcultured as needed (2–3 times a week in a subcultivation ratio of 1:5 to 1:8) and harvested from flasks using 0.25% (w/v) trypsin-EDTA. HeLa cells were seeded into a white wall clear bottom 384-well plate in 30 μL at a density of 3000 cells/well. Then, cells were grown for 48 h under standard conditions (37 °C and 5% CO_2) before adding ND@Au-Tf nanoparticles at a final amount of approximately 2×10^{11} (240 μg of particles per 1 mL) in tetraplicates. After 24 h of treatment with or without nanoparticles, the medium was removed, and the cells were thoroughly washed with fresh medium (three times). Then, the medium in each well was replaced with PBS, and selected wells were illuminated immediately (Ti:Sapphire laser – 75 MHz, 750 nm, pumped at 532 nm by ND:YAG, laser power of 2.1W, spot diameter of 2.7 mm, irradiation time of 60 sec). After irradiation, PBS was replaced with a fresh complete growth medium (30 μL), and the plate was incubated for an additional 24 h before viability measurement. Cell viability was determined using the CellTiter-Glo Luminescent Cell Viability Assay (Promega, Madison, WI, USA), which is based on quantification of the ATP present in cell lysates, according to the manufacturer's protocol. Briefly, the 384-well plate and its contents were equilibrated at room temperature for 30 min. CellTiter-Glo reagent was prepared by reconstituting the lyophilized enzyme/substrate mixture with CellTiter-Glo buffer equilibrated to room temperature. After an equal volume of CellTiter-Glo reagent was added to the wells (30 μL), the plate was shaken for 2 min on an orbital shaker (500 RPM) to induce cell lysis. Luminescence was recorded after an additional 10 min incubation in the dark using the multimode microplate reader Tecan Infinite M1000 (Tecan Austria GmbH, Grödig, Austria). Blank wells (containing medium without cells) were measured for luminescence and deducted from the values obtained from experimental wells (background luminescence). The viability values of treated cells were expressed as percentages of the values obtained for the corresponding control cells. Values (of the luminescent signal) represent the mean ± S.D. of four replicates obtained from two independent experiments.

Figures:

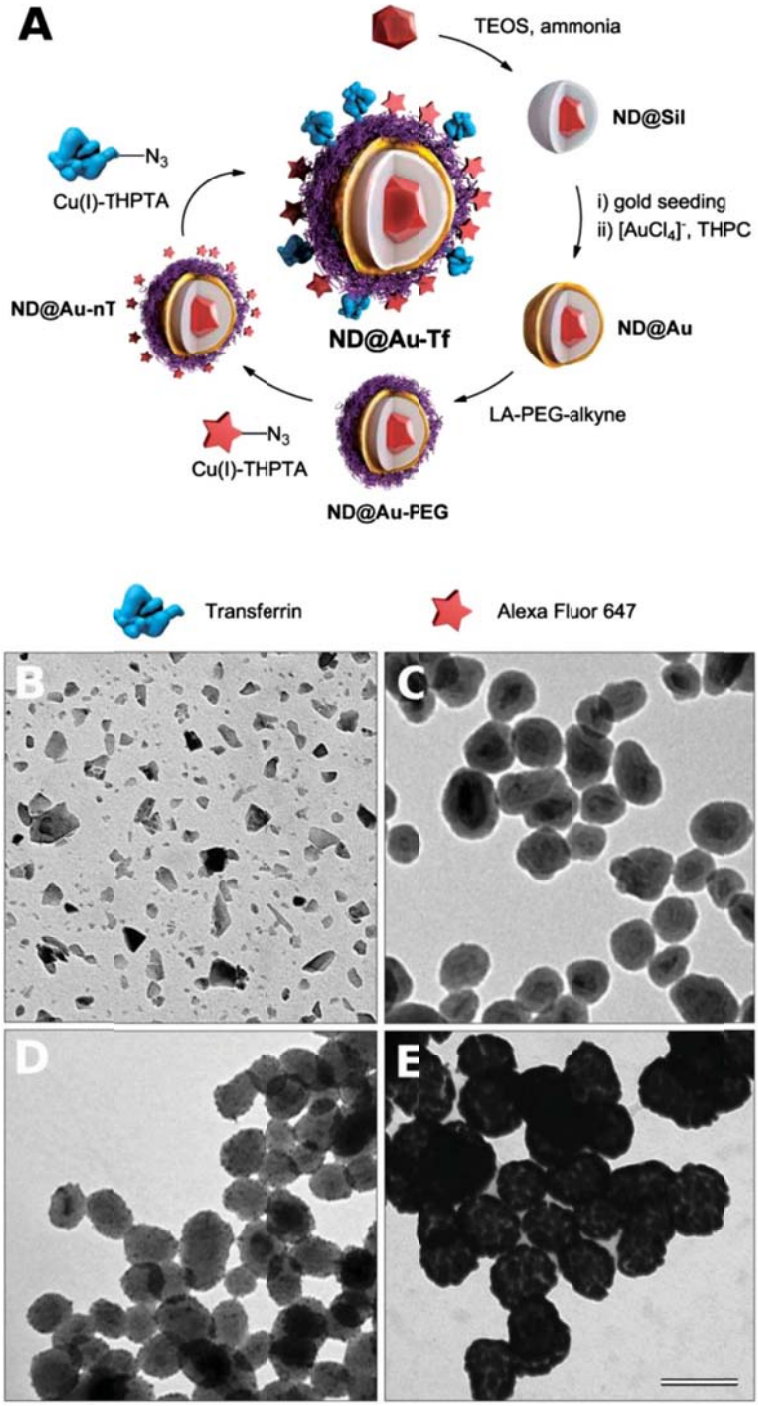

Figure 1. (A) Schematic representation of the preparation of GNSs with a diamond core. First, a silica shell is created on diamond particles, followed by formation of a GNS upon reduction of [AuCl 4]$^{-}$ promoted by adsorbed gold nanoparticle seeds. The GNS is modified with a lipoic acid- PEG conjugate, which is terminated with an alkyne. Using click chemistry, Alexa Fluor 647 dye and azide-modified transferrin (the targeting protein) are attached in consecutive steps. (B–D) TEM microphotographs of (B) diamond particles, (C) silica-coated diamond particles (ND@Sil), (D) silica-coated diamond particles with gold seeds, and (E) GNSs a with diamond core (ND@Au). The magnification is the same for all microphotographs, and the scale bar corresponds to 100 nm.

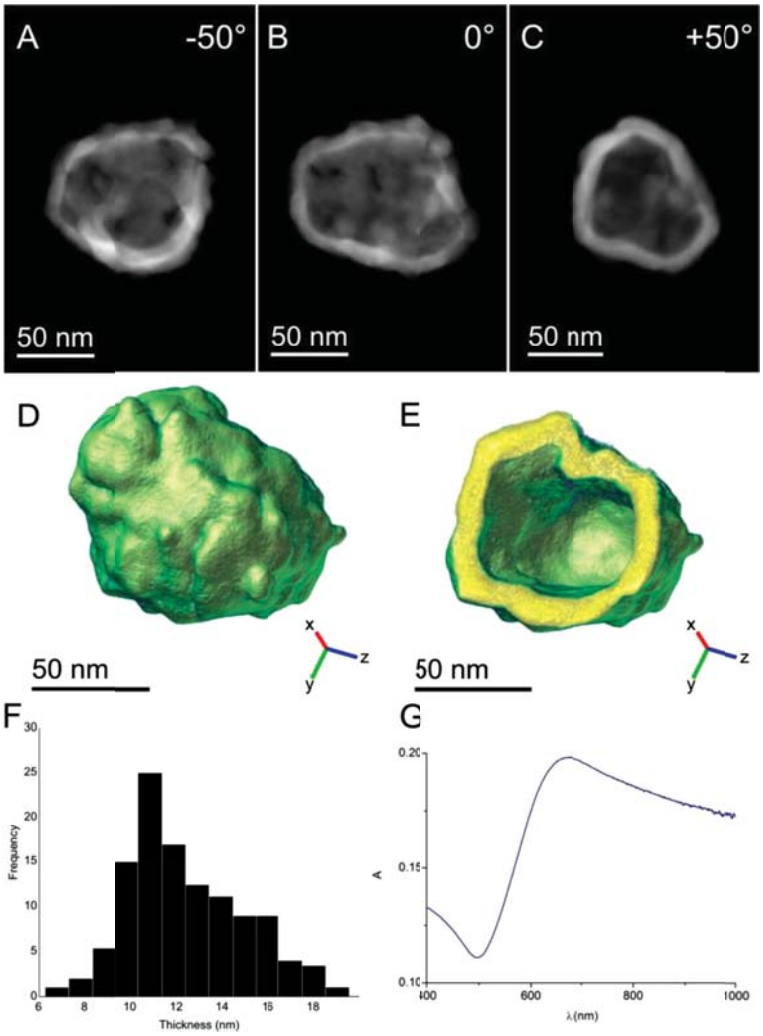

Figure 2. (A–C) 2D HAADF-STEM projections of a ND-silica particle coated with a GNS (ND@Au) obtained at different tilt angles. The diamond core and silica coating are not visible due to the limited dynamic range of the image detector. (D) A 3D representation of the reconstructed nanoshell. (E) A slice through the 3D reconstruction of the GNS demonstrating the homogeneity of shell thickness. (F) A histogram indicating the measured thicknesses of the shell based on electron tomography reconstruction. The average shell thickness was 12.6 ±0.3 nm. (G) Absorption spectrum of ND@Au in water at 15 μg/mL concentration (which corresponds to a ND concentration of 0.5 μg/mL).

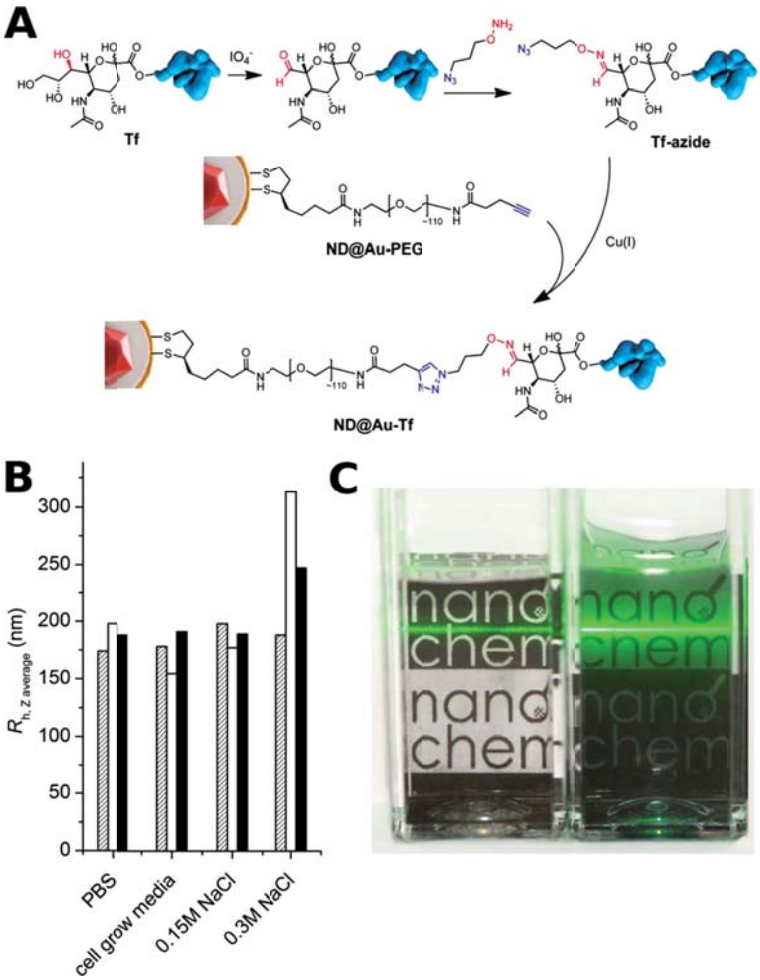

Figure 3. Structure of ND@Au-PEG conjugate and its colloidal stability in aqueous solutions with high ionic strength. A) Composition of the particle surface architecture after modification and attachment of Tf. B) Hydrodynamic radii of ND@Au-PEG in various solutions after 1 h (hatched), 1 week (white) and 1 month (black), showing no aggregation. C) Photograph of naked (ND@Au , left) and PEG-coated (ND@Au-PEG , right) particles dispersed in PBS (20 min after mixing; 0.2 mg/mL concentration). The precipitating ND@Au particles are already partially sedimented on the bottom of the vial, while the remaining large aggregates unevenly scatter the laser beam. The ND@Au-PEG particles form a stable colloidal solution, which evenly and strongly scatters the laser beam.

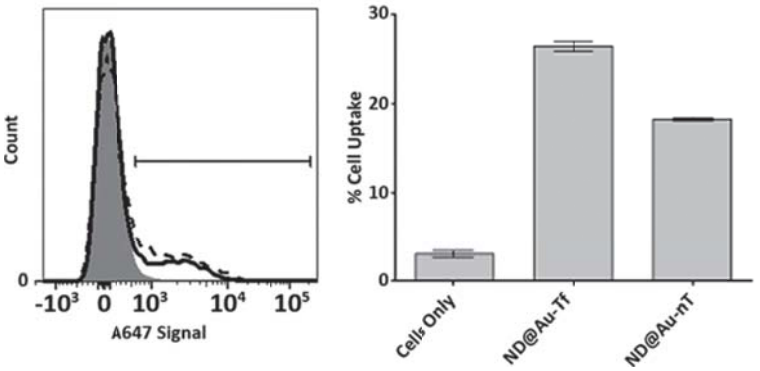

Figure 4. SKBR3 cell interactions with particles determined by flow cytometry. Left histogram: gray, cells only; dashed, ND@Au-Tf ; solid, ND@Au-nT . Right graph: Statistical analysis showing percent cellular uptake (positive cells shown on histogram by gate) for each sample. Error bars indicate standard deviation. Experiments were conducted in triplicate, and 10 000 gated events were analyzed. Student's t -test indicates significant differences comparing targeted ND@Au-Tf and non-targeted ND@Au-nT formulations ($p < 0.05$).

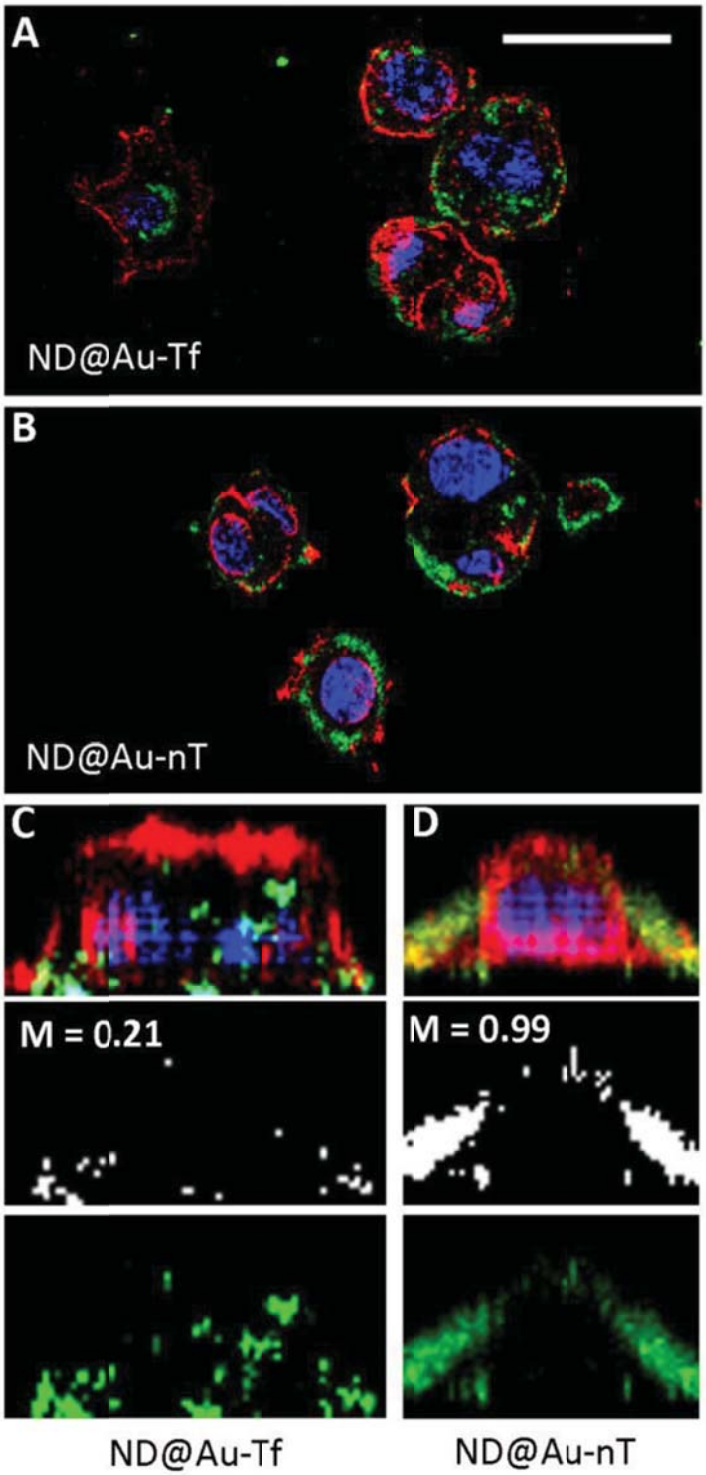

Figure 5. SKBR3 cell interactions with particles observed by confocal microscopy. The particles were incubated with SKBR3 cells for 16 h, fi xed, stained, and imaged. ND@Au-Tf (A+C) and ND@Au-nT (B+D) are pseudo-colored in green (imaged based on the Alexa Fluor 647 label), nuclei are shown in blue (stained with DAPI), and cell membranes are shown in red (stained with WGA-A555); the scale bar is 30 μm. C+D shows 3D reconstruction of single cells: the top panel shows all channels, the middle panel depicts co-localization of the particles and WGA signals (M =Mander's coefficient of co-localization determined using ImageJ software), and the bottom panel shows ND signals.

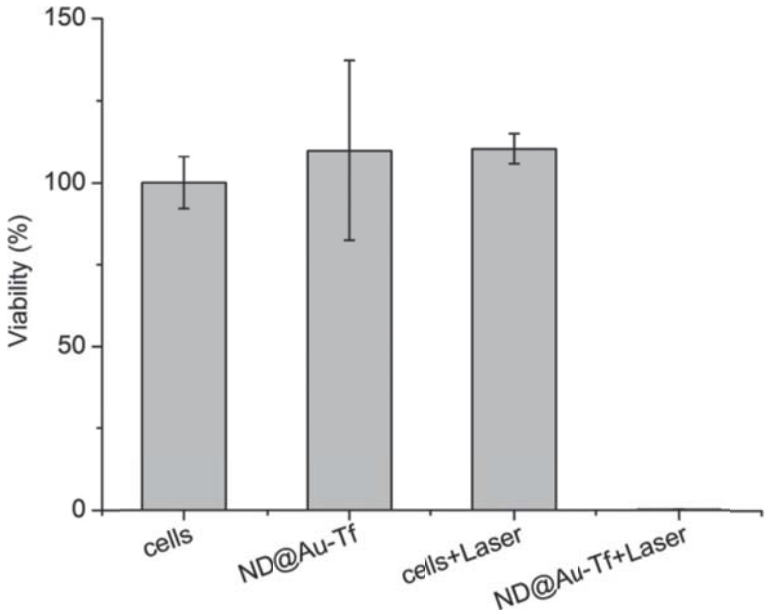

Figure 6. Laser ablation of HeLa cells incubated with ND@Au-Tf nanoparticles. Cell viability was estimated by luciferase assay with 24 h delay after 1 min irradiation with 37 W/cm^2 intensity. The viability of cells treated with ND@Au-Tf and laser was ≈0.15%.

References:

1. Khlebtsov, N. G. & Dykman, L. A. Optical properties and biomedical applications of plasmonic nanoparticles. *J. Quant. Spectrosc. Radiat. Transf.* **111,** 1–35 (2010).

2. Jones, M. R., Osberg, K. D., Macfarlane, R. J., Langille, M. R. & Mirkin, C. A. Templated Techniques for the Synthesis and Assembly of Plasmonic Nanostructures. *Chem. Rev.* **111,** 3736–3827 (2011).

3. Daniel, M. C. & Astruc, D. Gold nanoparticles: assembly, supramolecular chemistry, quantum-size-related properties, and applications toward biology, catalysis, and nanotechnology. *Chem. Rev.* **104,** 293–346 (2004).

4. Henry, A.-I. *et al.* Correlated Structure and Optical Property Studies of Plasmonic Nanoparticles. *J. Phys. Chem. C* **115,** 9291–9305 (2011).

5. Agrawal, A. *et al.* Quantitative evaluation of optical coherence tomography signal enhancement with gold nanoshells. *J. Biomed. Opt.* **11,** 041121–041121–8 (2006).

6. Kah, J. C. Y. *et al.* Concentration dependence of gold nanoshells on the enhancement of optical coherence tomography images: a quantitative study. *Appl. Opt.* **48,** D96–D108 (2009).

7. Chen, Y.-S. *et al.* Silica-Coated Gold Nanorods as Photoacoustic Signal Nanoamplifiers. *Nano Lett.* **11,** 348–354 (2011).

8. Stern, J. M., Stanfield, J., Kabbani, W., Hsieh, J.-T. & Cadeddu, J. A. Selective Prostate Cancer Thermal Ablation With Laser Activated Gold Nanoshells. *J. Urol.* **179,** 748–753 (2008).

9. Lu, W. *et al.* Targeted Photothermal Ablation of Murine Melanomas with Melanocyte-Stimulating Hormone Analog–Conjugated Hollow Gold Nanospheres. *Clin. Cancer Res.* **15,** 876–886 (2009).
10. Huang, X., El-Sayed, I. H., Qian, W. & El-Sayed, M. A. Cancer Cell Imaging and Photothermal Therapy in the Near-Infrared Region by Using Gold Nanorods. *J. Am. Chem. Soc.* **128,** 2115–2120 (2006).
11. Wu, G. *et al.* Remotely Triggered Liposome Release by Near-Infrared Light Absorption via Hollow Gold Nanoshells. *J. Am. Chem. Soc.* **130,** 8175–8177 (2008).
12. Bardhan, R. *et al.* Nanosphere-in-a-Nanoshell: A Simple Nanomatryushka. *J. Phys. Chem. C* **114,** 7378–7383 (2010).
13. Bardhan, R., Lal, S., Joshi, A. & Halas, N. J. Theranostic Nanoshells: From Probe Design to Imaging and Treatment of Cancer. *Acc. Chem. Res.* **44,** 936–946 (2011).
14. Gobin, A. M. *et al.* Near-Infrared Resonant Nanoshells for Combined Optical Imaging and Photothermal Cancer Therapy. *Nano Lett.* **7,** 1929–1934 (2007).
15. Hui, Y. Y., Cheng, C. L. & Chang, H. C. Nanodiamonds for optical bioimaging. *J. Phys. Appl. Phys.* **43,** 374021 (2010).
16. Badea, I. & Kaur, R. Nanodiamonds as novel nanomaterials for biomedical applications: drug delivery and imaging systems. *Int. J. Nanomedicine* 203–220 (2013). doi:10.2147/IJN.S37348
17. Lim, T.-S. *et al.* Fluorescence enhancement and lifetime modification of single nanodiamonds near a nanocrystalline silver surface. *Phys. Chem. Chem. Phys.* **11,** 1508–1514 (2009).
18. Chi, Y., Chen, G., Jelezko, F., Wu, E. & Zeng, H. Enhanced Photoluminescence of Single-Photon Emitters in Nanodiamonds on a Gold Film. *IEEE Photonics Technol. Lett.* **23,** 374–376 (2011).
19. Schietinger, S., Barth, M., Aichele, T. & Benson, O. Plasmon-Enhanced Single Photon Emission from a Nanoassembled Metal−Diamond Hybrid Structure at Room Temperature. *Nano Lett.* **9,** 1694–1698 (2009).
20. Barth, M., Schietinger, S., Schröder, T., Aichele, T. & Benson, O. Controlled coupling of NV defect centers to plasmonic and photonic nanostructures. *J. Lumin.* **130,** 1628–1634 (2010).
21. Yung Hui, Y. *et al.* Tip-enhanced sub-diffraction fluorescence imaging of nitrogen-vacancy centers in nanodiamonds. *Appl. Phys. Lett.* **102,** 013102–013102 (2013).
22. Chen, G. *et al.* Photoluminescence Enhancement Dependent on the Orientations of Single NV Centers in Nanodiamonds on a Gold Film. *IEEE J. Sel. Top. Quantum Electron.* **19,** 4602404–4602404 (2013).
23. Rehor, I. *et al.* Fluorescent Nanodiamonds with Bioorthogonally Reactive Protein-Resistant Polymeric Coatings. *ChemPlusChem* **79,** 21–24 (2014).
24. Zhang, B. *et al.* Photoacoustic emission from fluorescent nanodiamonds enhanced with gold nanoparticles. *Biomed. Opt. Express* **3,** 1662–1629 (2012).

25. Ismaili, H. & Workentin, M. S. Covalent diamond–gold nanojewel hybrids via photochemically generated carbenes. *Chem. Commun.* **47,** 7788 (2011).
26. Cheng, L.-C. *et al.* Targeting polymeric fluorescent nanodiamond-gold/silver multi-functional nanoparticles as a light-transforming hyperthermia reagent for cancer cells. *Nanoscale* **5,** 3931–3940 (2013).
27. Liu, Y. L. & Sun, K. W. Plasmon-enhanced photoluminescence from bioconjugated gold nanoparticle and nanodiamond assembly. *Appl. Phys. Lett.* **98,** 153702 (2011).
28. Rehor, I. *et al.* Fluorescent Nanodiamonds Embedded in Biocompatible Translucent Shells. *Small* (2014). doi:10.1002/smll.201302336
29. Howarth, M. *et al.* Monovalent, reduced-size quantum dots for imaging receptors on living cells. *Nat. Methods* **5,** 397–399 (2008).
30. Banerjee, D., Liu, A. P., Voss, N. R., Schmid, S. L. & Finn, M. G. Multivalent Display and Receptor-Mediated Endocytosis of Transferrin on Virus-Like Particles. *ChemBioChem* **11,** 1273–1279 (2010).
31. Mei, B. C. *et al.* Modular poly(ethylene glycol) ligands for biocompatible semiconductor and gold nanocrystals with extended pH and ionic stability. *J. Mater. Chem.* **18,** 4949–4958 (2008).
32. Susumu, K., Mei, B. C. & Mattoussi, H. Multifunctional ligands based on dihydrolipoic acid and polyethylene glycol to promote biocompatibility of quantum dots. *Nat. Protoc.* **4,** 424–436 (2009).
33. Mohan, N., Chen, C.-S., Hsieh, H.-H., Wu, Y.-C. & Chang, H.-C. In Vivo Imaging and Toxicity Assessments of Fluorescent Nanodiamonds in Caenorhabditis elegans. *Nano Lett.* **10,** 3692–3699 (2010).
34. Vaijayanthimala, V. *et al.* The long-term stability and biocompatibility of fluorescent nanodiamond as an in vivo contrast agent. *Biomaterials* **33,** 7794–7802 (2012).
35. Graf, C., Vossen, D. L. J., Imhof, A. & van Blaaderen, A. A General Method To Coat Colloidal Particles with Silica. *Langmuir* **19,** 6693–6700 (2003).
36. Rasch, M. R., Sokolov, K. V. & Korgel, B. A. Limitations on the Optical Tunability of Small Diameter Gold Nanoshells. *Langmuir* **25,** 11777–11785 (2009).
37. Oldenburg, S. ., Averitt, R. ., Westcott, S. . & Halas, N. . Nanoengineering of optical resonances. *Chem. Phys. Lett.* **288,** 243–247 (1998).
38. Brinson, B. E. *et al.* Nanoshells Made Easy: Improving Au Layer Growth on Nanoparticle Surfaces. *Langmuir* **24,** 14166–14171 (2008).
39. Hong, V., Presolski, S. I., Ma, C. & Finn, M. G. Analysis and Optimization of Copper-Catalyzed Azide-Alkyne Cycloaddition for Bioconjugation. *Angew. Chem. Int. Ed.* **48,** 9879–9883 (2009).
40. Prokop, A. & Davidson, J. M. Nanovehicular intracellular delivery systems. *J. Pharm. Sci.* **97,** 3518–3590 (2008).
41. Presolski, S. I., Hong, V. P. & Finn, M. G. in *Curr. Protoc. Chem. Biol.* (Arkin, A. P. et al.) (John Wiley & Sons, Inc., 2011). at <http://doi.wiley.com/10.1002/9780470559277.ch110148>

42. Bernardi, R. J., Lowery, A. R., Thompson, P. A., Blaney, S. M. & West, J. L. Immunonanoshells for targeted photothermal ablation in medulloblastoma and glioma: an in vitro evaluation using human cell lines. *J. Neurooncol.* **86,** 165–172 (2008).

Supporting Information

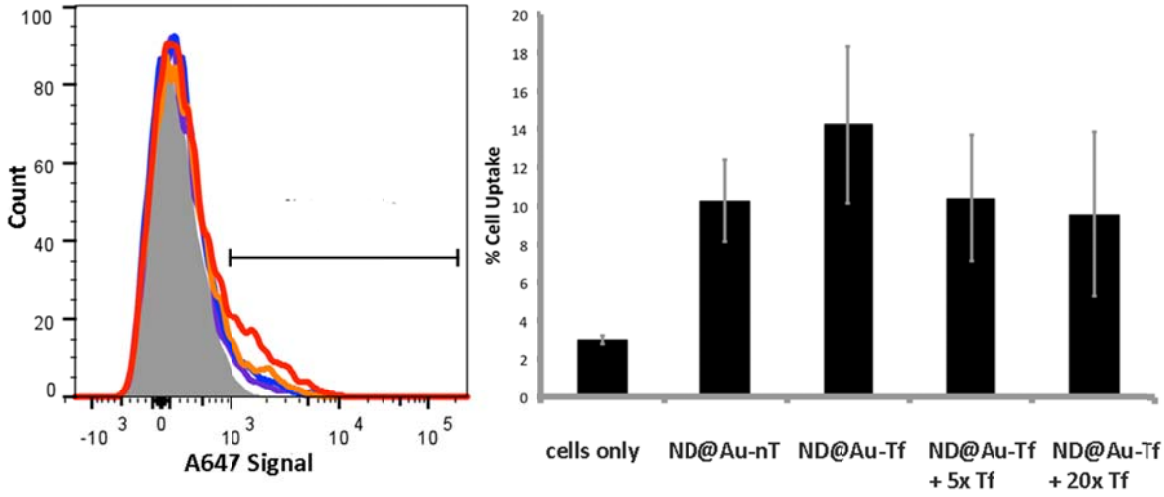

Figure S1: Nanodiamond-cell interactions using SKBR3 cells determined by flow cytometry – competition binding assay. Left: Histograms: gray = cells only; red = **ND@Au-Tf**; orange = **ND@Au-nT**; blue = competition 5x free Tf; purple = competition 20x free Tf. Right: Statistical analysis showing percent cellular uptake (positive cells shown on histogram by gate) for each sample. Error bars indicate mean ± standard deviation. Experiments were conducted in triplicate, and 10,000 gated events were analyzed.

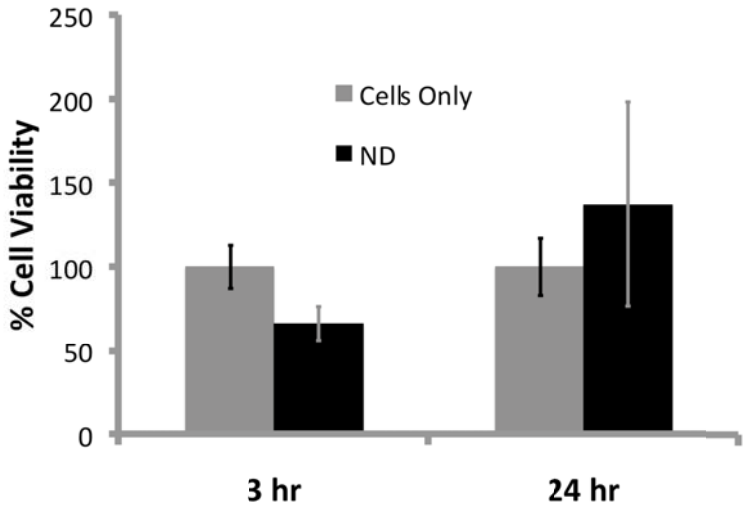

Figure S2: Cell viability of SKBR3 after expose to ND@Au-Tf. **ND@Au-Tf** (black) were incubated with SKBR3 cells for 3 and 24 hours. Percent cell viability was evaluated using an XTT assay and compared to a cells only control (gray). Toxicity is not indicated. Although reduced cell viability was indicated for cells exposed to **ND@Au-Tf** for a 3-hour time frame, toxic effects were not statically significant, neither were toxic effects observed at longer exposure times (24 hours).